Planetary Nebulae: A Universal Toolbox in the Era of Precision Astrophysics Proceedings IAU Symposium No. 384, 2025
O. De Marco, A. Zijlstra & R. Szczerba, eds. doi:10.1017/S1743921324000103

Dust formation in AGB stars and planetary nebulae

Mikako Matsuura

Cardiff Hub for Astrophysical Research and Technology (CHART), School of Physics and Astronomy, Cardiff University, The Parade, Cardiff CF24 3AA, UK

Abstract. A high sensitivity and high-angular resolutions infrared space telescope, the James Webb Space Telescope (JWST), allowed us to study dust and molecules in unprecedented details. This contribution highlights the first year of JWST's scientific operation, and reports prospects of dust and molecular studies in the coming future.

Keywords. (ISM:) dust, extinction; infrared: stars; (ISM:) planetary nebulae: general; stars: AGB and post-AGB

1. Introduction

The circumstellar envelopes of asymptotic giant branch (AGB) stars are considered to be important dust formation sites. They have a reasonably high density ($>10^{10}\,\mathrm{cm^{-3}}$) and warm ($\sim 1000\,\mathrm{K}$) gas at the inner region of the circumstellar envelope, which enables reasonably fast chemical reactions (e.g. Cherchneff 2012). Once the stars leave the AGB phase, their circumstellar envelopes are irradiated by strong UV from the central star of the planetary nebula (PN). UV radiation can cause post-formation processing of dust, changing the properties of the grains. In general, a diverse range of dust species have been detected in AGB stars, post-AGB stars and PNe. The detected species of dust grains include amorphous and crystalline silicates, SiC, and polycyclic aromatic hydrocarbons (PAHs), though PAHs might be considered to be large molecules rather than dust grains.

As the near- and mid-infrared spectral range covers a wide range of dust features, the near- and mid-infrared James Webb Space Telescope (JWST) (Gardner et al. 2023) is an excellent telescope to study dust grains in AGB stars and PNe. At the time of this IAU symposium, JWST has completed just over one year of scientific operations, and some highlights from its first year of operation are reported.

2. Highlights of JWST observations of PNe

2.1. NGC 3132: H₂ clumps and dusty disk

On 12th July 2022, the Space Telescope Science Insitute (STScI) released the first scientific images and spectra, taken by JWST (Gardner et al. 2023). One of the four targets of the first scientific data release was PN NGC 3132, showing the stunning detailed structures of this PN (Fig 1). The left-side image of Fig 1 is taken by NIRCam (Rieke et al. 2023) in six filter bands: F090W, F187N, F212N, F356W, F405N and F470N. The ionised gas, traced by [S III] in the F090W band and Pa α in the F187N band, is enclosed within the blue elliptical nebula, and is surrounded by clumps and filaments of H₂ in orange-red colour (De Marco et al. 2022). The right-side image of Fig 1 shows a MIRI (Wright et al. 2023) image of the nebula, taken in four filter bands (F770W, F1130W, F1280W and F1800W). Similar to the NIRCam image, H₂ filaments and clumps, which are in blue

[©] The Author(s), 2025. Published by Cambridge University Press on behalf of International Astronomical Union. This is an Open Access article, distributed under the terms of the Creative Commons Attribution licence (https://creativecommons.org/licenses/by/4.0/), which permits unrestricted re-use, distribution and reproduction, provided the original article is properly cited.

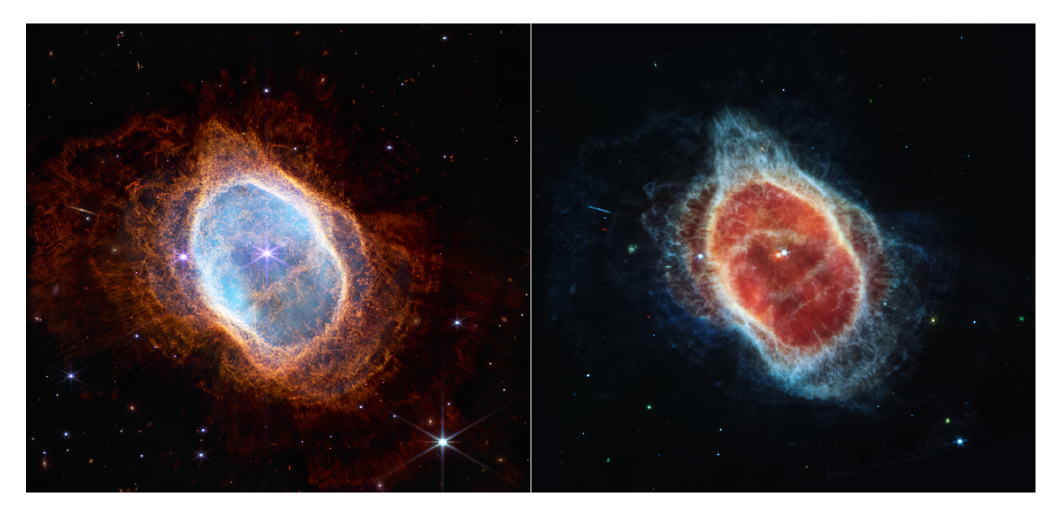


Figure 1. JWST images of NGC 3132, taken by the NIRCam (left) and the MIRI (right). The image is from the JWST Early Release Observations (Pontoppidan et al. 2022). Image credit: NASA, ESA, CSA, STScI.

and are traced by the F770W band, are found outside of the elliptically-shaped ionisation front in red. Although not too obvious in this press release image, there are layers of H_2 concentric arcs, surrounding the ionised gas, and H_2 spikes extending in a radial direction.

One of the surprising results is the detection of the mid-infrared excess from the central star of NGC 3132. Fig. 2 shows the image of the central star and its A-type star companion (De Marco et al. 2022). In the optical, the A-type companion is far brighter, but at wavelengths longer than $10 \,\mu\text{m}$, the central star is brighter. Moreover, the central star is not a point source, and is marginally resolved at these wavelengths, with an approximate size of 300 au in the full-width at half-maximum (FWHM). The fit to this mid-infrared excess (Fig. 3) shows that it is explained by a dust mass of $2 \times 10^{-7} \, M_{\odot}$, with an inner radius of 55 au. In order to retain such a quantity of AGB dust near the central star after the central star left the AGB phase approximately 10,000 years ago, the most likely explanation is that dust grains are trapped in a binary disk (Mastrodemos and Morris 1999).

In NGC 3132, H₂ emission is found in clumps (Fig. 4). That is similar to H₂ clumps found in the Helix Nebula (Meixner et al. 2005; Matsuura et al. 2007, 2009) and the Ring Nebula (this contribution). Fig. 4 shows the images of clumps found in NGC 3132 in three different regions (from top to bottom rows) at six different wavelengths (from right to left columns). Some clumps and filaments are seen in obscuration due to dust extinction in optical images taken by the *Hubble Space Telescope (HST)* in Fig. 4. Some clumps are even seen in absorption in the infrared NIRCam F187N and F405N images.

Using the dust extinction of clumps against the bright background nebular emission, clump masses can be estimated. We measured the extinction at 1.87 μ m for two clumps seen in extinction against the Pa α nebula background: the largest knot on the west side of the nebula (coordinates RA=10:07:00.4, Dec=-40:26:08.8), and one of the darkest on the east side of the nebula (RA=10:07:02.5, Dec=-40:26:00.3). The diameters of these clumps are ~0.36 arcsec and ~0.15 arcsec, and their extinction is ~0.57 mag and ~0.25 mag at 1.87 μ m, respectively. Using the dust extinction law $A(\lambda)/A(V)$, where $A(\lambda)$ is the extinction at a given wavelength, λ , and A(V) is the extinction in the V-band (Cardelli et al. 1989), the corresponding values of A(V) are 3.9 mag and 1.7 mag assuming $R_V = 3.1$. Using the conversion between A(V) and the total hydrogen density

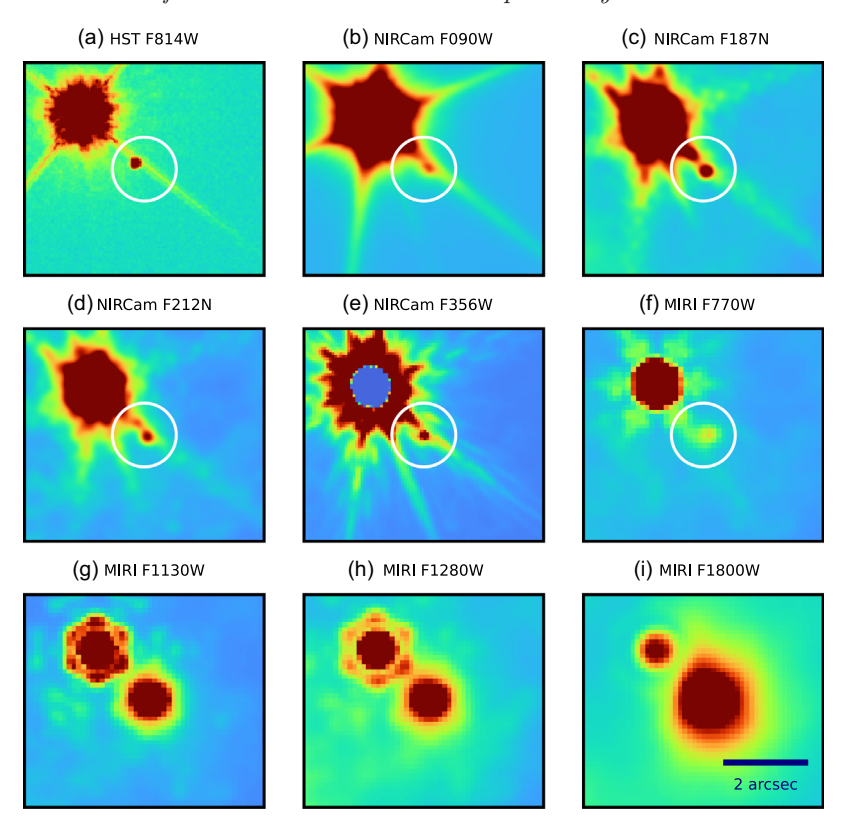


Figure 2. The multiple-wavelength images of the central star (white circle) and A-type companion star of NGC 3132. The companion star is far brighter in the optical, while in the mid-infrared wavelength range longer than F1130W, the central star is brighter, showing dust excess around the central star. The comparison with an A-type star shows that at F1130W, F1280W and F1800W, the central star is not a point source but extended. The figure is from De Marco et al. (2022).

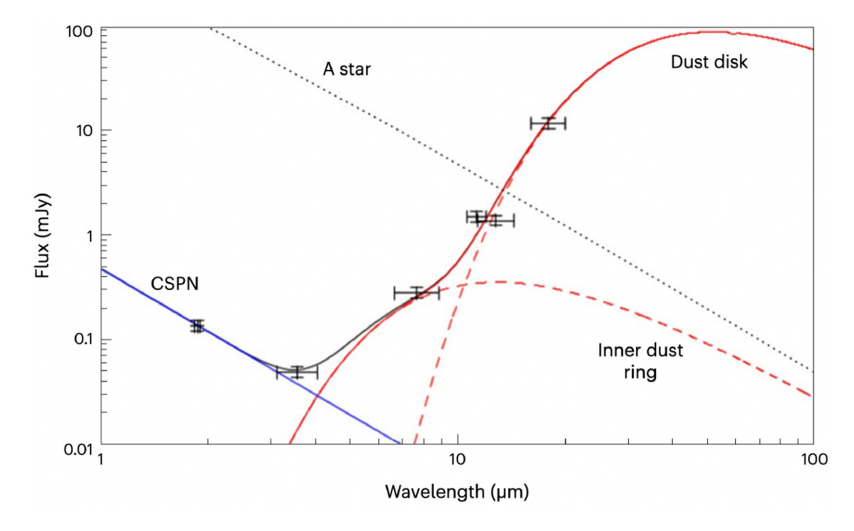


Figure 3. The spectral energy distribution of the central star of NGC 3132 and its dust disk, showing the dust excess, starting at about $3 \mu m$. The figure is from De Marco et al. (2022).

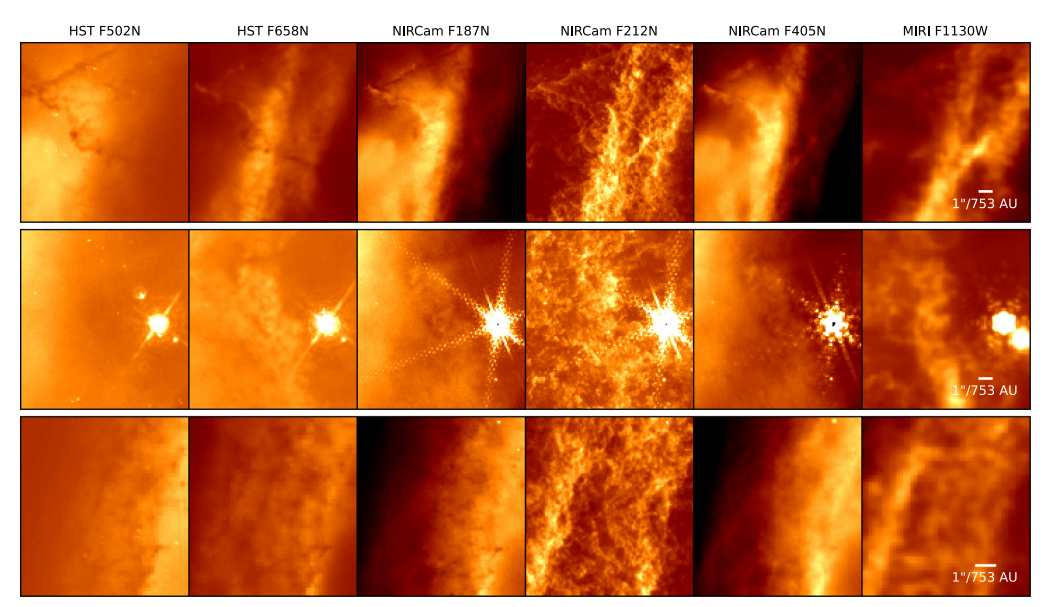


Figure 4. Enlarged images of clumps in three representative regions in NGC 3132: the west side of the ring (top row), near the centre of the ring (middle row) and the east side of the ring (bottom row). Filament structures stand out in the NIRCam F212N images. A few filaments are extinguished by dust, as clearly seen in the HST optical images (first two columns of HST F502N and F658N), but also even in infrared images at NIRCam F187N and F405N (third and fifth columns). The figure is from De Marco et al. (2022).

along the line of sight, N(H) (Bohlin et al. 1978), the estimated column densities of these two clumps are $N(H) = 7.3 \times 10^{21}$ cm⁻² and $N(H) = 3.2 \times 10^{21}$ cm⁻², respectively. For the adopted distance of 754 pc, the estimated densities are $n(H) \sim 2 \times 10^6$ cm⁻³ for both clumps. These densities suggest clump masses of $10^{-5} M_{\odot}$, similar to the typical clump ('globule') masses found in the Helix Nebula (Meixner et al. 2005; Matsuura et al. 2009). Considering the total number of clumps, there is about $0.1 M_{\odot}$ in the H₂ clumps (De Marco et al. 2022). A substantial fraction of the nebula mass is therefore in H₂.

2.2. The Ring Nebula: H₂ globules, radial spikes, and the PAH shell

JWST (Gardner et al. 2023) observed the Ring Nebula (M 57, NGC 6720) during Cycle 1 as part of the General Observers (GO) program 1558 (PI M.J. Barlow). Fig. 5 shows the NIRCam (left) and MIRI (right) false-colour images of the Ring Nebula. The main part of the nebula is filled with numerous clumps of H₂, shown in cyan (F212N), green (F300M) and red (F335M) colours in the NIRCam image. These clumps are also seen in the MIRI image in purple (F560W), blue (F770W) and cyan (F1000W) colours. The clumpy nebula is filled with ionised gas, traced in blue (F162M) in the NIRCam image and orange (F1800W, dominated by [S III]) in the MIRI image. A summary table of the main contributing emissions to each filter band is found in Wesson et al. (this contribution) and Wesson et al. (2023). On top of the clumpy structure of the main body of the nebula, the Ring Nebula shows up to 10 concentric arcs in H₂ and about 300–400 radial spikes (Wesson et al. 2023).

Compared with H_2 clumps detected in the Helix Nebula (Meixner et al. 2005; Matsuura et al. 2007, 2009) and NGC 3132 (De Marco et al. 2022), those detected in the Ring Nebula tend to have less defined heads or tails (Wesson et al. 2023). This is not due to the fact that the Ring Nebula (790 \pm 30 pc; Lindegren et al. 2021) is farther than

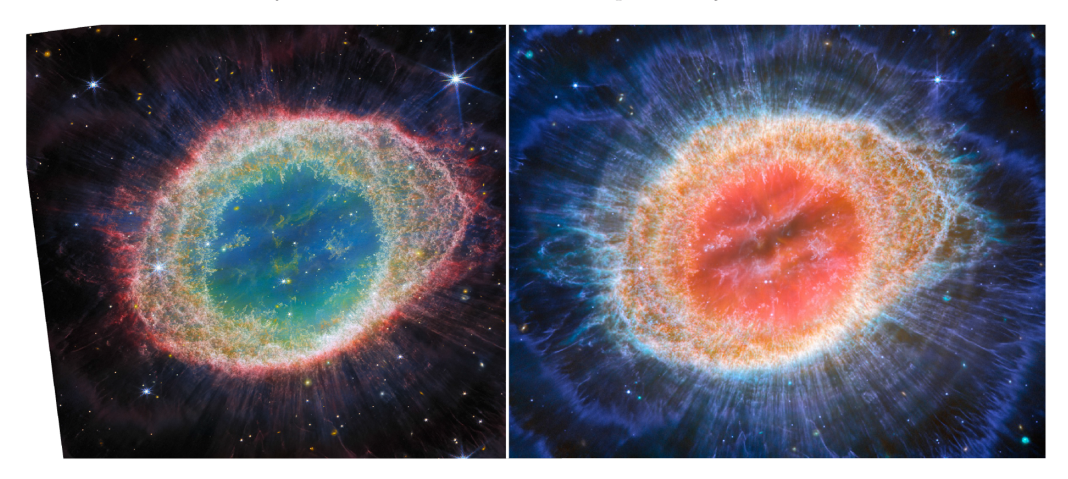


Figure 5. JWST images of the Ring Nebula, taken by the NIRCam (left) and the MIRI (right). The images use the data from the General Observers (GO) program 1558 (Wesson et al. 2023). Credit: ESA/Webb, NASA, CSA, M. Barlow, N. Cox, R. Wesson

the Helix Nebula $(200\pm30\,\mathrm{pc};\ \text{Lindegren et al. 2021});\ \text{NGC 3132}$ has a similar distance $(750\,\mathrm{pc};\ \text{De Marco et al. 2022}).$ Instead, it is probably because the Ring Nebula has had a shorter time since its central star left the peak of its luminosity, and is less evolved.

Hydrodynamic models (García-Segura and Mac Low 1995; Garcia-Segura and Franco 1996) demonstrated that instabilities in existing gas layers being swept up can form clumpy structures. Initially, the range of clump sizes is quite uniform as found in the Ring Nebula, but as the nebula evolves, instabilities build up and tails gradually develop, so that the range of clump sizes grows, as found in NGC 3132 and the Helix Nebula.

JWST's high sensitivity and high angular resolution images of the Ring Nebula show a distinct thin shell, associated with PAHs, in the Ring Nebula. Fig. 6 includes intensity ratios of (a) F335M/F300M and (b) F1130W/F1000W. The F335M and F1130W filters contain PAH bands, while the F300M and F1000W filters include nearby continuum, though there are some weak line contributions, too (Wesson et al. 2023). Nevertheless, the similar thin shell morphology found in both F335M/F300M and F1130W/F1000W images shows that the thin shell represents the location of PAHs. Compared with the overall shell of the Ring, seen in the F212N H₂ image (Fig. 6 (d)), the PAH shell is located approximately at the edge of the main body of the Ring, which contains H₂ clumps.

Spitzer spectral mapping at 11.3 μ m is shown at Fig. 6 (c). This map is a single wavelength bin with a spectral resolution of $R \sim 100$ (Houck et al. 2004). The data were taken by Program 40536 (P.I. H. Dinerstein) and published by Cox et al. (2016). This spectral map covers the 11.3 μ m PAH band. The black circle, which traces the PAH emission in Fig. 6 (a) and (b) is also plotted in panel (c), and indeed, the PAH emission is strongest in region 3, where the black circle crosses.

Fig. 7 shows Spitzer spectra, extracted in the three regions, indicated in Fig. 6 (c). As expected, region 3 has a clear indication of the PAH band at $11.3\,\mu\mathrm{m}$, with region 2 having weak PAH emission. Regions 2 and 3 both show an excess of the F1130W over the F1000W flux, relative to a simply rising continuum, suggesting the presence of PAH emission in F1130W/F1000W. There is no trace of PAHs in the central ionised region 1. Region 1, the innermost region of the ring, lacks PAH emission at $11.3\,\mu\mathrm{m}$ but has strong [S IV] emission in the JWST F1000W filter. This confirms that the thin emission shell, found in F335M/F300M (Fig. 6 (a)) and F1130W/F1000W (Fig. 6 (b)), is indeed due to PAHs.

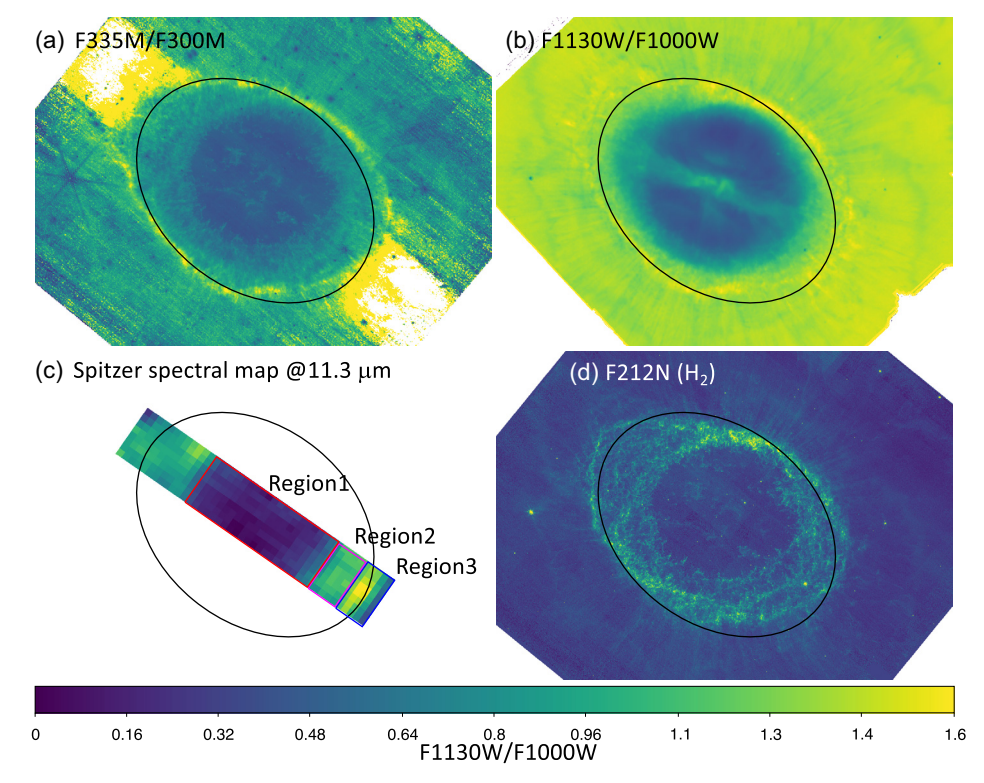


Figure 6. The PAH shell found in the Ring Nebula. The four panels show (a) F335M/F300M ratio, (b) F1130W/F1000W ratio and (c) Spitzer spectral map at $11.3 \,\mu\mathrm{m}$ ($10.95-11.65 \,\mu\mathrm{m}$, corresponding to JWST F1130W filter) (Cox et al. 2016) on the same scale. For reference, the black ellipse approximately traces the narrow ring at the edge of the shell, which is interpreted as the peak PAH emission. For comparison, the F212N H₂ image is plotted at the panel (d). The Spitzer spectra were extracted at three different regions as indicated in the bottom left panel, and plotted at Fig. 7. North is at the top. The figure is from Wesson et al. (2023)

The location of the PAH-emitting peak at the edge of the H₂ clumps is most likely due to favourable UV excitation of PAHs at this particular distance from the central star. As traced by a black ellipse in Fig. 6, the PAH shell is centred on the current location of the central star, rather than the offset centre found for other emission features, and follows the outer contour of the H₂ distribution (Wesson et al. 2023). As expected from Fig. 6 (d), the peak of H₂ is offset from the central star by about 2 arcsec (Wesson et al. 2023). This offset seems to be associated with the proper motion of the central star, since the nebula material was expelled from the central star about 4000 yrs ago (O'Dell et al. 2004). Although PAHs and H₂ are both associated with clumps, there is a difference in their brightness distributions; PAH brightness peaks are outside of H₂ brightness peaks, and PAH brightness is centred on the current position of the star, while the H₂ brightness is not. This strongly suggests that the PAH excitation, rather than PAH abundance or density distribution within the nebula, contributes to the presence of the PAH peaks.

2.3. Spectroscopic signature of dust in PN SMP LMC 058

Another early JWST result of dust in PNe came from the commissioning data of the MIRI spectrometer (Wright et al. 2023). SMP LMC 058 is a PN located in the Large Magellanic Cloud (LMC) which was initially identified by an emission source survey

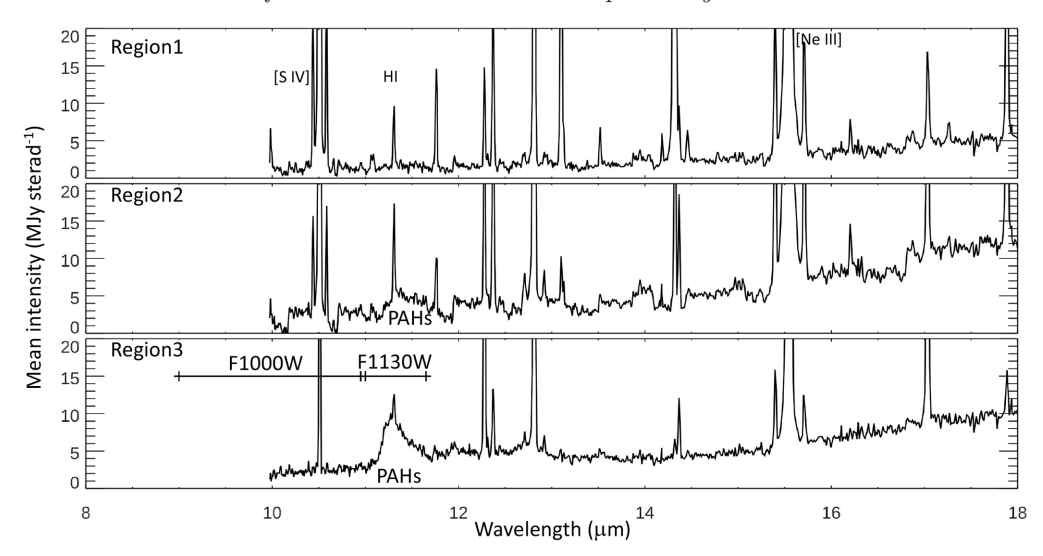


Figure 7. The extracted *Spitzer* spectra of the Ring Nebula (Cox et al. 2016), from the top towards the inner ring from regions 1 to 3. (bottom left panel of Fig. 6). Region 3 has an excess of PAHs at $11.3 \,\mu\text{m}$ in Figure 6, and *Spitzer* spectra confirm the presence of $11.3 \,\mu\text{m}$ PAHs. In contrast, region 1, the innermost region of the ring, lacks observed PAHs. The figure is from Wesson et al. (2023)

(Sanduleak et al. 1978). Spitzer IRS spectra (R = 60–127) have identified the SiC feature at 11.3 μ m. The PAH features at 6–9 μ m were identified, but the PAH feature at \sim 11.3 μ m was unclear (Bernard-Salas et al. 2009).

Higher spectral resolution (R=1500-4000) MIRI spectra clearly identified over 50 emission lines from the 4.9–27.9 μ m spectra of SMP LMC 058 (Fig.8; Jones et al. 2023). More relevant to this contribution is the detection of PAHs and SiC dust emissions at 11 μ m in this PN. With *Spitzer's* spectral resolution, it was difficult to disentangle contributions from the 11.3 μ m SiC, the 11.2 μ m PAHs, and the 11.3 μ m HI 9–7. On the other hand, the higher spectral resolution of MIRI was capable of disentangling these three components. Fig. 8 shows the identification of the broad ~11.3 μ m SiC. The SiC band is rarely to be found in Galactic high mass-loss rate AGB stars, post-AGB stars and PNe (Speck et al. 2005), while it is rather common in their LMC counterparts (Gruendl et al. 2008; Bernard-Salas et al. 2009; Matsuura et al. 2014; Sloan et al. 2014). On top of the broad SiC band, a narrower and fainter PAH 11.2 μ m is clearly detected in MIRI spectra (Fig. 8). That is the power of the higher spectral resolution of the MIRI spectrometer, compared with the *Spitzer* IRS in the low-spectral resolution mode.

2.4. End of the era of discrete C-rich and O-rich chemistry?

Finally, JWST discovered chemical processes related to dust formation in general, not specific to PNe, but very relevant to dust formation in PNe. The Solar abundance pattern indicates that the gas contains more oxygen than carbon atoms, and the majority of stars were formed from gas with more oxygen than carbon atoms. During the AGB phase, carbon atoms are synthesised and dredged up to the surface, and hence, surface abundances might show a carbon-to-oxygen ratio larger than unity.

In AGB stars, post-AGB stars and PNe, distinct C-rich or O-rich chemistry is operating, depending on which elemental abundance of oxygen or carbon is higher. In a chemical process, carbon monoxide (CO) has the highest binding energy among molecules, hence

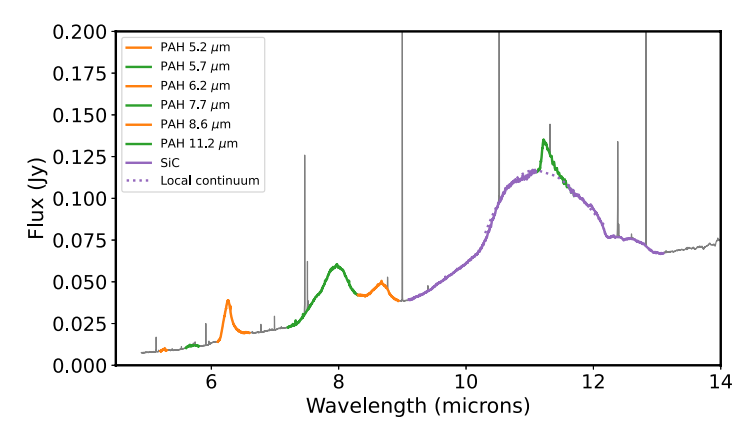


Figure 8. JWST/MIRI spectra of the PN, SMP LMC 058. The broad SiC band at 11.3μ is identified, and on top of that PAH 11.2μ m is found. Other PAH features, such as 5.2, 5.7, 6.2, 7.7 and 8.6μ m are also found. The figure is from Jones et al. (2023)

CO molecules are formed first in AGB stars, when the gas is sufficiently cool. In an oxygen-rich environment (C/O<1), the remaining oxygen atoms react with other atoms, forming H_2O , SiO, CO_2 and silicate dust (e.g. Mg_2SiO_4 , $MgSiO_3$). In a carbon-rich environment (C/O>1), the excess carbon atoms react with other atoms, producing molecules such as C_2H_2 , HCN, CS, CH, as well as carbonaceous dust (amorphous carbon, SiC and PAHs). Occasionally, molecules and dust which have been formed both in oxygen-rich and carbon-rich environments are found within a single object, and these objects are called dual chemistry objects. Often dual-chemistry objects show silicate dust with PAHs (e.g. Waters et al. 1998; Molster et al. 2002). Some PNe show oxygen-rich abundances from atomic line analysis, and yet also show PAHs. The prime example is the Ring Nebula. As discussed in Sect. 2.2, the Ring Nebula does present PAHs, which are carbon-rich molecules/dust, but its gas abundances were measured to be oxygen-rich from atomic lines (Liu et al. 2004).

There are several hypotheses on how to form dual chemistry objects. One possible explanation is that binary discs have been formed in AGB stars/post-AGB stars and PNe, and past oxygen-rich material has been stored in these discs (Waters et al. 1998; Winckel et al. 2006). The central star eventually became carbon-rich, and carbon-rich molecules and dust were formed in this later phase.

The hypothesis of storing oxygen-rich gas in binary-formed discs might work in AGB stars/post-AGB stars and PNe. However, PAHs are widely found in the diffuse interstellar medium (ISM), and their origin there is not clear, as the ISM gas is oxygen-rich. Another issue is that the mass of PAHs formed in AGB stars is expected to be far too small, compared with the mass found in the ISM in galaxies. In carbon-rich AGB stars, PAHs may be formed via combining C_2H_2 (Allamandola et al. 1989). However, the abundance of C_2H_2 is quite low, and even across the entire AGB population in the Small Magellanic Cloud (SMC), only $10^{-8} M_{\odot} \text{ yr}^{-1}$ of PAHs may be injected to the ISM (Matsuura et al. 2013). That would make only about $100 M_{\odot}$ of PAHs during the lifetime of PAHs in the ISM (1.4–1.6×10⁸ yr; Micelotta et al. 2010). On the other hand, Sandstrom et al. (2010) estimated the fractional abundance of PAHs in the SMC ISM to be 0.6 per cent with respect to the total dust mass. Considering the SMC dust mass of 8×10^4 – $5 \times 10^5 M_{\odot}$ (Gordon et al. 2014), the resultant PAH mass in the SMC ISM would be 500–3000 M_{\odot} . Though there are a lot of uncertainties involved in these estimates, AGB-injected PAHs seem to be insufficient to explain the whole PAH mass in the ISM.

In order to explain the large mass of PAHs found in the ISM, there is a long-term debate on whether PAHs may be formed within the ISM in situ, instead of being injected from AGB stars to the ISM. JWST opened clues to this hypothesis. Berné et al. (2023) reported the detection of CH⁺³, which has been predicted to trigger organic chemistry (Black and Dalgarno 1977), potentially leading to the formation of PAHs. That was detected in the proto-planetary disc d203–506 in the Orion Nebula. The proto-planetary disc is exposed to UV radiation from the Trapezium stars, and this strong UV ($G_0 > 10^4$) irradiation triggered the formation of CH⁺³, and subsequent organic molecule formation in this high density ($n > 10^5$ cm⁻³) region. Although the first detection of CH⁺³ was in a proto-planetary disc, the implication of this chemistry might be relevant to organic chemistry in the oxygen-rich environment in PNe (Berné et al. 2023).

Another finding from JWST was dual chemistry being detected in young stellar objects,. Tabone et al. (2023) reported the detection of C_2H_2 , C_6H_6 , CO_2 , C_4H_2 from a young (2.6±1.6 Myr old) low-mass star 2MASS J16053215-1933159. CO_2 forms in the oxygen-rich environment, while C_2H_2 , C_6H_6 and C_4H_2 are carbon-rich in origin. This star is a member of a star-forming region and has an accreting disc around it. One possible explanation is that oxygen atoms are frozen in H_2O ice, so the abundance of carbon-bearing molecules is higher. This has implications for AGB stars and PNe. Some high-mass loss rate AGB stars can have ice (Justtanont et al. 2006), so ice-induced carbon-chemistry might be applicable to evolved stars, too. Future investigations in AGB stars, post-AGB stars and PNe will be important.

Acknowledgements

This work is based on observations made with the NASA/ESA/CSA James Webb Space Telescope. The data were obtained from the Mikulski Archive for Space Telescopes at the Space Telescope Science Institute, which is operated by the Association of Universities for Research in Astronomy, Inc., under NASA contract NAS 5-03127 for JWST. These observations are associated with program #1558.

M.M. acknowledges support from STFC Consolidated grant (ST/W000830/1).

References

- Allamandola, L. J., Tielens, A. G. G. M., & Barker, J. R. 1989, Interstellar polycyclic aromatic hydrocarbons - The infrared emission bands, the excitation/emission mechanism, and the astrophysical implications. Astrophysical Journal Supplement Series (ISSN 0067-0049), 71, 733-775.
- Bernard-Salas, J., Peeters, E., Sloan, G. C., Gutenkunst, S., Matsuura, M., Tielens, A. G. G. M., Zijlstra, A. A., & Houck, J. R. 2009, UNUSUAL DUST EMISSION FROM PLANETARY NEBULAE IN THE MAGELLANIC CLOUDS. *The Astrophysical Journal*, 699(2), 1541–1552.
- Berné, O., Martin-Drumel, M.-A., Schroetter, I., Goicoechea, J. R., Jacovella, U., Gans, B., Dartois, E., Coudert, L. H., Bergin, E., Alarcon, F., Cami, J., Roueff, E., Black, J. H., Asvany, O., Habart, E., Peeters, E., Canin, A., Trahin, B., Joblin, C., Schlemmer, S., Thorwirth, S., Cernicharo, J., Gerin, M., Tielens, A., Zannese, M., Abergel, A., Bernard-Salas, J., Boersma, C., Bron, E., Chown, R., Cuadrado, S., Dicken, D., Elyajouri, M., Fuente, A., Gordon, K. D., Issa, L., Kannavou, O., Khan, B., Lacinbala, O., Languignon, D., Gal, R. L., Maragkoudakis, A., Meshaka, R., Okada, Y., Onaka, T., Pasquini, S., Pound, M. W., Robberto, M., Röllig, M., Schefter, B., Schirmer, T., Sidhu, A., Tabone, B., Putte, D. V. D., Vicente, S., & Wolfire, M. G. 2023, Formation of the methyl cation by photochemistry in a protoplanetary disk. Nature, 1–4.
- Black, J. H. & Dalgarno, A. 1977, Models of interstellar clouds. I The Zeta Ophiuchi cloud. The Astrophysical Journal Supplement Series, 34, 405.

- Bohlin, R. C., Savage, B. D., & Drake, J. F. 1978, A survey of interstellar H I from L-alpha absorption measurements. II. *Astrophysical Journal*, 224, 132. A&AA ID. AAA022.131.015.
- Cardelli, J. A., Clayton, G. C., & Mathis, J. S. 1989, The relationship between infrared, optical, and ultraviolet extinction. *Astrophysical Journal*, 345, 245.
- Cherchneff, I. 2012, The inner wind of IRC+ 10216 revisited: new exotic chemistry and diagnostic for dust condensation in carbon stars. A & A, 545, A12.
- Cox, N. L. J., Pilleri, P., Berne, O., Cernicharo, J., & Joblin, C. 2016, Polycyclic aromatic hydrocarbons and molecular hydrogen in oxygen-rich planetary nebulae: the case of NGC 6720. MNRAS, 456(1), L89–L93.
- De Marco, O., Akashi, M., Akras, S., & et al. 2022, The messy death of a multiple star system and the resulting planetary nebula as observed by JWST. *Nature Astronomy*, 6(12), 1421–1432.
- Garcia-Segura, G. & Franco, J. 1996, From Ultracompact to Extended H II Regions. ApJ, 469, 171.
- García-Segura, G. & Mac Low, M.-M. 1995, Wolf-Rayet Bubbles. II. Gasdynamical Simulations. ApJ, 455, 160.
- Gardner, J. P., Mather, J. C., Abbott, R., & et al. 2023, The James Webb Space Telescope Mission. PASP, 135(1048), 068001.
- Gordon, K. D., Roman-Duval, J., Bot, C., Meixner, M., Babler, B., Bernard, J.-P., Bolatto, A. D., Boyer, M. L., Clayton, G. C., Engelbracht, C., Fukui, Y., Galametz, M., Galliano, F., Hony, S., Hughes, A., Indebetouw, R., Israel, F. P., Jameson, K., Kawamura, A., Lebouteiller, V., Li, A., Madden, S. C., Matsuura, M., Misselt, K., Montiel, E., Okumura, K., Onishi, T., Panuzzo, P., Paradis, D., Rubio, M., Sandstrom, K. M., Sauvage, M., Seale, J., Sewiło, M., Tchernyshyov, K., & Skibba, R. 2014, Dust and gas in the Magellanic Clouds from the Heritage Herschelkey Project. I. Dust properties and insights into the origin of the submillimeter excess emission. The Astrophysical Journal, 797(2), 85.
- Gruendl, R. A., Chu, Y.-H., Seale, J. P., Matsuura, M., Speck, A. K., Sloan, G. C., & Looney, L. W. 2008, Discovery of Extreme Carbon Stars in the Large Magellanic Cloud. The Astrophysical Journal, 688(1), L9–L12. (c) 2008: The American Astronomical Society.
- Houck, J. R., Roellig, T. L., van Cleve, J., & et al. 2004, The Infrared Spectrograph (IRS) on the Spitzer Space Telescope. *ApJS*, 154(1), 18–24.
- Jones, O. C., Álvarez-Márquez, J., Sloan, G. C., Kavanagh, P. J., Argyriou, I., Law, D. R., Labiano, A., Patapis, P., Mueller, M., Larson, K. L., Bright, S. N., Klaassen, P. D., Fox, O. D., Gasman, D., Geers, V. C., Glauser, A. M., Guillard, P., Nayak, O., Noriega-Crespo, A., Ressler, M. E., Sargent, B., Temim, T., Vandenbussche, B., & García Marín, M. 2023, Observations of the planetary nebula SMP LMC 058 with the JWST MIRI medium resolution spectrometer. MNRAS, 523(2), 2519–2529.
- Justtanont, K., Olofsson, G., Dijkstra, C., & Meyer, A. W. 2006, Near-infrared observations of water-ice in OH/IR stars. A&A, 450(3), 1051–1059.
- Lindegren, L., Bastian, U., Biermann, M., Bombrun, A., de Torres, A., Gerlach, E., Geyer, R., Hernández, J., Hilger, T., Hobbs, D., Klioner, S. A., Lammers, U., McMillan, P. J., Ramos-Lerate, M., Steidelmüller, H., Stephenson, C. A., & van Leeuwen, F. 2021, Gaia Early Data Release 3. Parallax bias versus magnitude, colour, and position. A&A, 649, A4.
- Liu, Y., Liu, X., Luo, S., & Barlow, M. J. 2004, Chemical abundances of planetary nebulae from optical recombination lines – I. Observations and plasma diagnostics. Monthly Notices of the Royal Astronomical Society, 353(4), 1231–1250.
- Mastrodemos, N. & Morris, M. 1999, Bipolar Pre–Planetary Nebulae: Hydrodynamics of Dusty Winds in Binary Systems. II. Morphology of the Circumstellar Envelopes. *Astrophysical Journal*, 523(1), 357–380.
- Matsuura, M., Bernard-Salas, J., Evans, T. L., Volk, K. M., Hrivnak, B. J., Sloan, G. C., Chu, Y.-H., Gruendl, R., Kraemer, K. E., Peeters, E., Szczerba, R., Wood, P. R., Zijlstra, A. A., Hony, S., Ita, Y., Kamath, D., Lagadec, E., Parker, Q. A., Reid, W. A., Shimonishi, T., Winckel, H. V., Woods, P. M., Kemper, F., Meixner, M., Otsuka, M., Sahai, R., Sargent, B. A., Hora, J. L., & McDonald, I. 2014, Spitzer Space Telescope spectra of post-AGB stars in the Large Magellanic Cloud polycyclic aromatic hydrocarbons at low metallicities.

- Monthly Notices of the Royal Astronomical Society, 439(2), 1472–1493.
- Matsuura, M., Speck, A. K., McHunu, B. M., Tanaka, I., Wright, N. J., Smith, M. D., Zijlstra, A. A., Viti, S., & Wesson, R. 2009, A "Firework" of H₂ Knots in the Planetary Nebula NGC 7293 (The Helix Nebula). ApJ, 700(2), 1067–1077.
- Matsuura, M., Speck, A. K., Smith, M. D., Zijlstra, A. A., Viti, S., Lowe, K. T. E., Redman, M., Wareing, C. J., & Lagadec, E. 2007, VLT/near-infrared integral field spectrometer observations of molecular hydrogen lines in the knots of the planetary nebula NGC 7293 (the Helix Nebula). MNRAS, 382(4), 1447–1459.
- Matsuura, M., Woods, P. M., & Owen, P. J. 2013, The global gas and dust budget of the Small Magellanic Cloud. Monthly Notices of the Royal Astronomical Society, 429(3), 2527–2536.
- Meixner, M., McCullough, P., Hartman, J., Son, M., & Speck, A. 2005, The Multitude of Molecular Hydrogen Knots in the Helix Nebula. AJ, 130(4), 1784–1794.
- Micelotta, E. R., Jones, A. P., & Tielens, A. G. G. M. 2010, Polycyclic aromatic hydrocarbon processing in interstellar shocks. Astronomy and Astrophysics, 510, A36.
- Molster, F. J., Waters, L. B. F. M., Tielens, A. G. G. M., & Barlow, M. J. 2002, Crystalline silicate dust around evolved stars. I. The sample stars. Astronomy and Astrophysics, 382, 184.
- O'Dell, C. R., McCullough, P. R., & Meixner, M. 2004, Unraveling the Helix Nebula: Its Structure and Knots. AJ, 128(5), 2339–2356.
- Pontoppidan, K. M., Barrientes, J., Blome, C., & et al. 2022, The JWST Early Release Observations. ApJ, 936(1), L14.
- Rieke, M. J., Kelly, D. M., Misselt, K., & et al. 2023, Performance of NIRCam on JWST in Flight. *PASP*, 135(1044), 028001.
- Sandstrom, K. M., Bolatto, A. D., Draine, B. T., Bot, C., & Stanimirović, S. 2010, The Spitzer Survey of the Small Magellanic Cloud (S3MC): Insights into the Life Cycle of Polycyclic Aromatic Hydrocarbons. The Astrophysical Journal, 715, 701.
- Sanduleak, N., MacConnell, D. J., & Philip, A. G. D. 1978, The planetary nebula systems of the Magellanic Clouds. PASP, 90, 621–635.
- Sloan, G. C., Lagadec, E., Zijlstra, A. A., Kraemer, K. E., Weis, A. P., Matsuura, M., Volk, K. M., Peeters, E., Duley, W. W., Cami, J., Bernard-Salas, J., Kemper, F., & Sahai, R. 2014, Carbon-rich Dust Past the Asymptotic Giant Branch: Aliphatics, Aromatics, and Fullerenes in the Magellanic Clouds. Astrophysical Journal, 791(1), 28.
- Speck, A. K., Thompson, G. D., & Hofmeister, A. M. 2005, The Effect of Stellar Evolution on SiC Dust Grain Sizes. The Astrophysical Journal, 634, 426. (c) 2005: The American Astronomical Society.
- Tabone, B., Bettoni, G., Dishoeck, E. F. v., Arabhavi, A. M., Grant, S., Gasman, D., Henning, T., Kamp, I., Güdel, M., Lagage, P. O., Ray, T., Vandenbussche, B., Abergel, A., Absil, O., Argyriou, I., Barrado, D., Boccaletti, A., Bouwman, J., Garatti, A. C. o., Geers, V., Glauser, A. M., Justannont, K., Lahuis, F., Mueller, M., Nehmé, C., Olofsson, G., Pantin, E., Scheithauer, S., Waelkens, C., Waters, L. B. F. M., Black, J. H., Christiaens, V., Guadarrama, R., Morales-Calderón, M., Jang, H., Kanwar, J., Pawellek, N., Perotti, G., Perrin, A., Rodgers-Lee, D., Samland, M., Schreiber, J., Schwarz, K., Colina, L., Östlin, G., & Wright, G. 2023, A rich hydrocarbon chemistry and high C to O ratio in the inner disk around a very low-mass star. Nature Astronomy, 7(7), 805–814.
- Waters, L. B. F. M., Jong, T. d., Molster, F. J., Loon, J. T. v., Bouwman, J., Koter, A. D., Waelkens, C., Winckel, H. V., Morris, P. W., Cami, J., & Graauw, T. d. 1998, An oxygenrich dust disk surrounding an evolved star in the Red Rectangle. *Nature*, 391, 868.
- Wesson, R., Matsuura, M., Zijlstra, A. A., & et al. 2023, JWST observations of the Ring Nebula (NGC 6720): I. Imaging of the rings, globules, and arcs. arXiv e-prints, arXiv:2308.09027.
- Winckel, H. V., Evans, T. L., Reyniers, M., Deroo, P., & Gielen, C. 2006, Binary post-AGB stars and their Keplerian discs. *Memorie della Societa Astronomica Italiana*, 77, 943. (c) 2006; SAIt.
- Wright, G. S., Rieke, G. H., Glasse, A., & et al. 2023, The Mid-infrared Instrument for JWST and Its In-flight Performance. *PASP*, 135(1046), 048003.